

Empty electronic states at the (100), (110), and (111) surfaces of nickel, copper, and silver

A. Goldmann

Laboratorium für Festkörperphysik der Universität, D-4100 Duisburg, Germany

V. Dose

Physikalisches Institut der Universität, Am Hubland, D-8700 Würzburg, Germany

G. Borstel

Fachbereich Physik der Universität, D-4500 Osnabrück, Germany

(Received 24 April 1985)

We have performed a systematic investigation of empty electronic surface states on the (100), (110), and (111) faces of nickel, copper, and silver using momentum-resolved inverse photoemission spectroscopy at $\hbar\omega=9.7$ eV. We present the measured two-dimensional energy-band dispersions $E(k_{\parallel})$ and discuss common trends. All the observed surface bands can be classified as being either crystal induced or image-potential induced. The former class of surface states is well known from ordinary photoemission and occurs in bulk band gaps as a consequence of the termination of the three-dimensional crystal periodicity. Image-potential states arise from the long-range forces which describe the screening of an electron approaching a metal surface by the conduction electrons and have no filled counterpart. The relationship between the two kinds of states can be qualitatively understood in terms of a one-dimensional model proposed by Echenique and Pendry. Numerical calculations are necessary for quantitative understanding. Comparison of the experimental data to such calculations is made where available. We conclude that the systematics of unoccupied *sp*-like surface states on fcc transition metals are now well established.

I. INTRODUCTION

The introduction of a surface to a solid breaks its three-dimensional symmetry, changes the coordination number of the surface atoms as compared to atoms in the bulk, and may therefore give rise to various modifications of the geometrical and electronic structure. To be specific, periodicity of the wave function in the *z* direction normal to the surface is no longer required and the resulting different boundary conditions for the wave functions give rise to the existence of electron states forbidden in the solid. Such states are called surface states or surface resonances, depending on their detailed physical origin. Angle-resolved photoemission^{1,2} has revealed a considerable number of occupied surface bands and determined their energy-dispersion and symmetry character. In particular, copper has provided an ideal test case for comparison between photoemission results and first-principles calculations of bulk and surface electronic structure.³ Much less is known about empty surface bands on metals. Only recently has the development of angle-resolved inverse photoemission spectroscopy⁴⁻⁷ made empty energy bands located between the vacuum level E_V and the Fermi energy E_F accessible to detailed investigations.

We have used this technique for a systematic study of the (100), (110), and (111) faces of Ni, Cu, and Ag. In the present paper we focus on our observation of empty surface bands and discuss obvious common features. Comparison is made to numerical energy-band calculations where available. The results for normal electron incidence will be explained qualitatively within a one-dimensional

multiple-reflection model for surface states developed by McRae, and Echenique and Pendry.⁸ This model is introduced in Sec. II. Our experimental results are presented in Sec. III. The discussion in Sec. IV leads us to conclude that *sp*-like surface bands obey general trends on fcc metal surfaces and that the underlying principles are rather well understood. In the case of Ni, Cu, and Ag, quantitative agreement between experiment and theory can be achieved to the same degree of accuracy as for bulk bands.⁹⁻¹² Energies generally agree to better than 1 eV and predicted band curvatures usually reproduce the experimental results quite well. The situation is different, however, for image-potential surface states.⁸ These states are intimately connected to the long-range behavior of the effective surface-potential barrier. The failure of the theory to predict accurate energies for image-potential states and bulk-gap-derived surface states simultaneously is not at all surprising. All calculations available at present use a rectangular-shaped barrier placed at typically less than one interlayer distance outside the outermost atomic layer. Clearly, improved barrier models must be treated in future theoretical work.

In the present paper the discussion is limited to ideal, well-ordered, unreconstructed surfaces. This has the important consequence that k_{\parallel} , the component of the wave vector parallel to the surface, is a well defined quantum number. We will therefore not consider localized surface states due to lattice defects, steps, or adsorbed atoms. Under these assumptions it has become customary in the literature to distinguish two kinds of surface states, classified as so-called Tamm states^{13,14} or Shockley states,¹⁵⁻¹⁹

depending on their conceptual origin. Tamm surface states are split off into a gap from bulk bands by the surface potential. Their existence requires that the surface perturbation of the one-electron potential be sufficiently strong compared with the bandwidth. They may be visualized in a simplified picture as a band-bending effect over the distance of one atomic layer. Shockley surface states occur in energy gaps caused by the hybridization of crossed bands, e.g., in *sp* gaps for which the lower band has odd symmetry at the zone boundary, while the upper band is even ("Shockley inverted" gap). In the noninverted case, with the upper state odd and the lower state even, gap states cannot exist due to the impossibility of wave matching at the surface.^{18,19} Shockley-type states are created if the surface potential draws away charge from the bulk and accumulates it in the surface state located in real space outside the atom cores—this is in fact the physical reason for the "inversion" of the critical-point ordering. Shockley inverted gaps are observed in Ni, Cu, and Ag at *X* (X_4 - X_1 gap, in single-group notation) and at *L* (L_2 - L_1). Both gaps extend above the Fermi energy E_F and are therefore promising energy ranges for a search for unoccupied surface bands.

Occupied Tamm states as well as occupied Shockley states have been clearly identified in a considerable number of photoemission studies in recent years.¹⁻³ For example, it is now well established that occupied Shockley states exist on the (111) surfaces of the noble metals^{1-3,20} and their ordered and disordered alloys like, e.g., $\text{Cu}_3\text{Au}(111)$ (Ref. 21) or $\text{Cu}_{0.9}\text{Al}_{0.1}(111)$ (Ref. 22). Occupied Tamm states with *d*-like orbital character split off the *d* bands have been observed on Cu,^{3,20,23} Ag,²⁴ and Au,²⁵ and their energy dispersion with k_{\parallel} could be calculated—often before their experimental identification—with considerable precision.²⁶ In the present study we confine the discussion to *sp*-like unoccupied states. In Cu and Ag, the *d* bands are located well below E_F and cannot contribute. In Ni, the *d* orbitals extend slightly [about 0.16 eV (Ref. 10)] above E_F . Our experimental data show no indication of an unoccupied Tamm state at Ni surfaces.

II. SURFACE STATES AT $\bar{\Gamma}$

Although several numerical calculations of unoccupied surface states on metals are available (see the subsequent discussion in Sec. IV), we will now summarize very shortly the one-dimensional two-band model proposed earlier by Pendry and co-workers.^{8,19} In contrast to most of the detailed numerical studies, it offers the advantage of great simplicity and transparency when explaining the level position and symmetry of surface states found at $k_{\parallel}=0$ within (or near) band gaps.

Echenique and Pendry⁸ describe an electron normally incident on a solid surface and trapped in a previously unoccupied surface state as a wave which is repeatedly reflected between the crystal edge and the surface-barrier potential. If the amplitude of the reflectivity of the crystal edge *C* and the barrier potential *B* is represented by $r_C e^{i\phi_C}$ and $r_B e^{i\phi_B}$, respectively, then the total amplitude of the wave after an infinite number of reflections is⁸

$$\{1 - r_B r_C \exp[i(\phi_C + \phi_B)]\}^{-1}. \quad (1)$$

Here, r and ϕ are the relevant reflection coefficients and phase changes, respectively. A pole in (1) denotes a surface state. The conditions for the existence of a surface state are therefore

$$r_B = r_C = 1 \quad (2)$$

and

$$\phi_C + \phi_B = 2\pi n, \quad (3)$$

where n is an integer. Clearly, condition (2) can only be met in a bulk band gap ($r_C=1$) and for total energies below the vacuum level ($r_B=1$). Such a case is depicted in Fig. 1(a), which characterizes the situation along the normal direction of a Cu(100) surface. The effective potential for an electron incident on the copper surface is the image-charge potential $V_B(z) \propto -(4z)^{-1}$ at large distances, a repulsive barrier at $z=0$, and a physically reasonable connection between the two at intermediate z . Condition (3) may be met by a rapid variation with energy of either ϕ_B or ϕ_C . Depending on which phase contributes predominantly to the total phase change, we follow Echenique and Pendry⁸ and distinguish "barrier-induced" image-potential states and "crystal-induced" gap states. Clearly, the phase condition, Eq. (3), is exact in a one-dimensional surface-potential model. The problem is that due to the generally unknown z dependence of the potential, neither ϕ_B nor ϕ_C are known precisely.

Nevertheless, the asymptotic behavior may be predicted reliably using plausible physical assumptions. If the surface barrier is continued in perfect Coulomb form up to $z=0$,

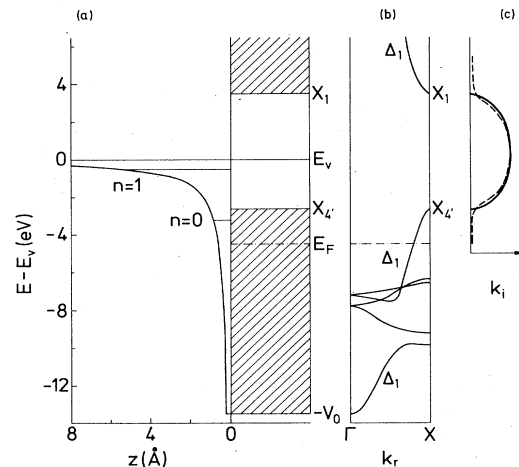


FIG. 1. (a) Schematic potential diagram for an image-potential surface state ($n=1$) on Cu(100), indicating the image-potential barrier $V_B(z)$ outside the crystal ($z > 0$) and the bulk band gap between X_4 and X_1 . (b) Bulk-band structure of Cu along ΓX , corresponding to normal electron incidence as a function of the real part k_r of the electron \mathbf{k} vector, and (c) the imaginary part k_i of \mathbf{k} inside the gap without (solid line) and with (dashed line) damping of the bulk states.

$$V_B(z) \propto -(4z)^{-1}, \quad z > 0 \\ = +\infty, \quad z < 0 \quad (4)$$

then ϕ_B may be estimated as²⁷

$$\phi_B/\pi = \left[\frac{3.4 \text{ eV}}{E_V - E} \right]^{1/2} - 1. \quad (5)$$

Neglecting ϕ_C altogether in Eq. (3), in the zeroth-order approximation, the lowest roots of (5) corresponding to $n=0, 1$ are $E_V - E = 3.4$ and 0.4 eV. The infinite number of roots for $n \geq 2$ falls in the range $0.4 \text{ eV} > E_V - E \geq 0$. Thus, the Rydberg-series-like infinite number of surface states predicted for $n \geq 1$ spans only a very narrow range of energies. This series will generally appear less than about 1 eV below E_V at $\bar{\Gamma}$ as one unresolved peak or step given the present-day experimental resolution.

Clearly, upon approaching the vacuum level ($n \rightarrow \infty$) the total phase is dominated by the behavior of ϕ_B . However, the neglect of ϕ_C is not at all justified for the $n=0$ state. In the following we try to estimate ϕ_C . Inspection of Fig. 1(b) suggests that we neglect the presence of the d bands located about 4 eV below X_4' and treat the $X_4' - X_1$ gap as in a nearly-free-electron case, where the wave functions near the gap edges can be represented by a linear combination of plane waves $e^{\pm ik_r z}$, where k_r is the real part of the wave vector along ΓX . Using this two-band-model approximation,^{16,18,28,29} the evanescent wave function in the gap may be written inside the crystal ($z < 0$) as

$$\Psi(z) = e^{ik_i z} \cos(k_X z + \delta). \quad (6)$$

Here, $k_X = 2\pi/a$ is the real part of \mathbf{k} on the zone boundary and the corresponding imaginary part k_i is given by¹⁸

$$k_i^2 = -E - (2\pi/a)^2 + [4E(2\pi/a)^2 + V_G^2]^{1/2}. \quad (7)$$

E is measured relative to the bottom of the inner (crystal) potential well, $2|V_G|$ is the width of the $X_4' - X_1$ gap, a is the lattice constant, and $\hbar^2/2m = 1$ in Eq. (7). The behavior of k_i is indicated in Fig. 1(c) by the solid line. The dashed line shows k_i after adding an imaginary part of $0.05V_G$ to the pseudopotential in order to simulate damping due to excited-state lifetime effects.³⁰ Figure 1(c) demonstrates that k_i remains nearly unaffected. Damping inside the gap will, however, introduce a small transmission probability into the crystal, and thus $r_C < 1$. In consequence, the surface state attains some finite lifetime broadening. This will not affect the basic ideas of the model. Note that $V_G > 0$ for the Shockley inverted case of Cu at X . Then the wave functions are $\propto \sin(k_X z)$ at X_4' and $\propto \cos(k_X z)$ at X_1 . The phase δ appearing in Eq. (6) varies then by $\pi/2$ across the gap. Wave matching at $z=0$ of (5) to the solution at $z > 0$ gives^{18,28} that, in the first-order approximation,

$$\phi_C \approx 2\delta. \quad (8)$$

Thus, ϕ_C changes by π from the bottom to the top of the energy gap and can contribute significantly to Eq. (3).

The foregoing discussion suggests the following conclusions:

(1) Near E_V , typically between E_V and 1 eV below E_V , we expect a Rydberg-like series of image-potential states at $\bar{\Gamma}$. In the approximation of Eq. (4),

$$E_V - E_n = 0.85 \text{ eV}/(n+a)^2, \quad (9)$$

where $\phi_C = \text{const}$ across the interval $|E_V - E_n| \leq 0.85 \text{ eV}$ was assumed and the quantum defect varies in the range $0 \leq a \leq \frac{1}{2}$, depending on ϕ_C . This result is not sensitive to the precise functional form of $V(z)$ if $n > 1$.

(2) The wave functions corresponding to $n \geq 1$ will extend far out into the vacuum. Their general behavior will be independent of the particular surface-atom geometry, provided a gap is available near E_V .

(3) Away from $\bar{\Gamma}$ the kinetic energy of the motion parallel to the surface has to be added and the lateral dispersion of the image-potential states will be

$$E(\mathbf{k}_{\parallel}) = E_V - E_n + \hbar^2 k_{\parallel}^2 / 2m^*, \quad (10)$$

where the effective mass m^* will in general depend on n .

(4) The precise energy position at $\bar{\Gamma}$ of the $n=0$ state will depend critically on the knowledge of both ϕ_C and ϕ_B for small z ; the corresponding wave function will be located in the immediate vicinity of the surface. This suggests the appellation "crystal induced." However, the general discussion of the matching conditions at $z=0$ (Refs. 8, 18, and 28) indicates that the $n=0$ state will always appear near the bottom of the gap. Depending on whether it will be located above or below E_F , it may be empty or occupied, respectively. If the $n=0$ solution of Eq. (3) shifts the crystal-induced state below the lower gap edge, it must be considered as a surface resonance rather than a true surface state. Such a situation is indicated in Fig. 1(a).

(5) All surface states ($n \geq 0$) predicted at $\bar{\Gamma}$ will have wave functions totally symmetric with respect to the surface normal.

III. EXPERIMENTAL RESULTS

All results reported in this paper are obtained by taking angle-resolved inverse photoemission spectra in the isochromat mode. Electrons with energy E_{kin} impinge on the sample at an angle θ with respect to the surface normal in a plane of well-defined azimuthal orientation. Spectra are obtained monitoring the emitted photon intensity at a fixed photon energy $\hbar\omega$ during a scan of E_{kin} . The experimental arrangement has been described in detail elsewhere.^{7,31} The photon spectrometer is based on an energy-selective ultraviolet Geiger-Müller counter which is iodine filled and has a CaF_2 entrance window. This combination of counting gas and window acts as a band-pass filter which detects photons at $\hbar\omega = 9.7 \text{ eV}$ with 0.8-eV overall resolution (full width at half maximum). In some cases, improved energy resolution was necessary in order to separate surface-band transitions from bulk-band transitions nearby. This was achieved by using a SrF_2 window at the entrance of the Geiger-Müller counter. The isochromat energy is then reduced to $\hbar\omega = 9.5 \text{ eV}$ and the resolution increases to $\Delta E = 0.4 \text{ eV}$, both at the expense of overall sensitivity.

We have systematically collected isochromat spectra in different azimuths from the (100), (110), and (111) sur-

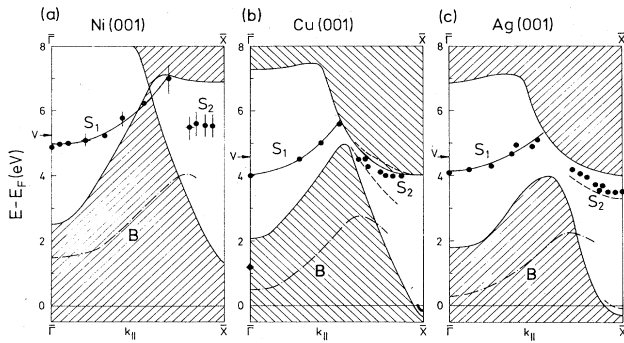


FIG. 2. Final-state energies $E(k_{\parallel})$ obtained at $\hbar\omega=9.7$ eV along the $\bar{\Gamma}\bar{X}$ direction of the surface Brillouin zone ($\bar{\Gamma}XUL$ bulk plane) of the (001) faces of (a) Ni, (b) Cu, and (c) Ag. S_1 represents image-potential states, S_2 crystal-derived surface bands. B labels observed bulk-interband transitions. The unshaded areas represent gaps of the projected bulk-band structures. The vacuum levels are indicated by arrows labeled V .

faces of Ni, Cu, and Ag. Representative sample spectra, which indicate the statistical quality of our data and the observed signal-to-noise ratio, have already been published elsewhere^{10,32,33} and need not be reproduced here. Several others will be published in due course^{34,35} and will be discussed in detail in the context of observed bulk-band transitions and adsorbate-derived features. All results relevant to the present discussion are condensed in the form of experimental $E(k_{\parallel})$ relations in Figs. 2–4. Figure 2 shows our data^{10,32,34} for electrons incident in the $\bar{\Gamma}XUL$ bulk mirror plane, i.e., along the $\bar{\Gamma}\bar{X}$ direction of the (100)-surface Brillouin zone.² The corresponding data along $\bar{\Gamma}\bar{M}'$ of the (111) surfaces are plotted in Fig. 3.^{10,34,35} Similarly, dispersion curves observed^{10,34,35} on (110) faces along the $\bar{\Gamma}\bar{X}$ and $\bar{\Gamma}\bar{Y}$ directions are presented in Fig. 4. The relation of the different surface-Brillouin-zone directions to the bulk $\bar{\Gamma}XUL$ mirror plane is defined in Fig. 5 and the inset of Fig. 4. In particular, Fig. 5 elucidates that $\bar{\Gamma}$ on (100) surfaces samples the $\bar{\Gamma}X$ direction of the

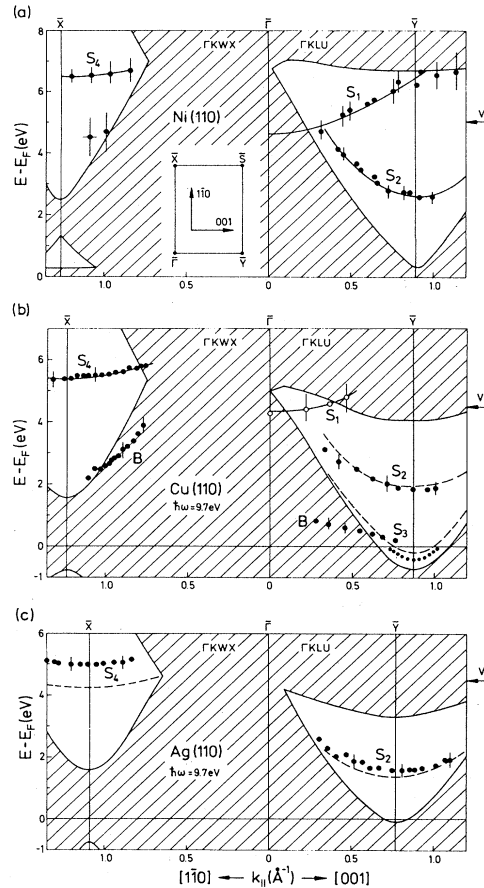


FIG. 4. Final-state energies $E(k_{\parallel})$ obtained at $\hbar\omega=9.7$ eV along the $\bar{\Gamma}\bar{X}$ and $\bar{\Gamma}\bar{Y}$ directions of the surface Brillouin zone of the (110) faces of (a) Ni, (b) Cu, and (c) Ag. S_1 indicates image-potential states and S_2 – S_4 , crystal-derived surface bands. B labels observed bulk-band transitions. The vacuum levels are given by arrows labeled V .

bulk, where a Shockley inverted $X_{4'}-X_1$ gap exists, see also Fig. 1(a). Similarly, \bar{X} on (100), $\bar{\Gamma}$ on (111), and \bar{Y} on (110) faces are all viewing (different) projections of the $L_{2'}-L_1$ Shockley inverted gap at L .

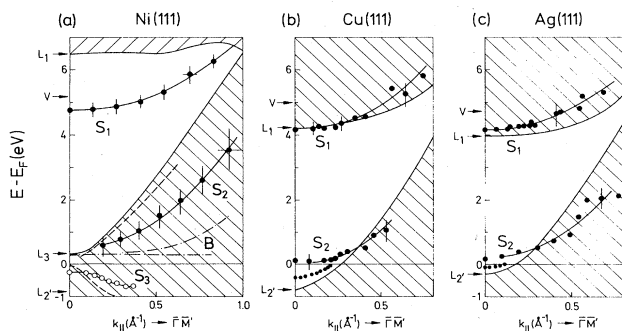


FIG. 3. Final-state energies $E(k_{\parallel})$ obtained at $\hbar\omega=9.7$ eV along the $\bar{\Gamma}\bar{M}'$ direction of the surface Brillouin zone of the (111) surfaces of (a) Ni, (b) Cu, and (c) Ag. S_1 labels image-potential states, S_2 and S_3 crystal-derived surface bands, and B observed bulk-interband transitions. The unshaded area are the gaps of the projected bulk bands. Vacuum levels are indicated by arrows labeled V .

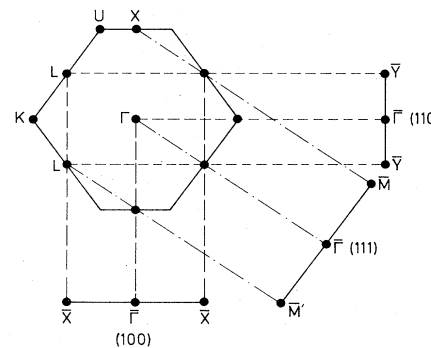


FIG. 5. Cross section through the bulk Brillouin zone showing the $\bar{\Gamma}XULK$ mirror plane of the fcc lattice and its projections on corresponding directions of the (100), (111), and (110) surface Brillouin zones.

In the identification of surface bands we have been guided by combinations of the following necessary criteria. A surface band should be sensitive to small amounts of surface contamination. Also it must be located in a gap of the projected bulk-band structure. In particular, $E(\mathbf{k}_\parallel)$ must be periodic with the periodicity of the surface Brillouin zone. Furthermore, a surface state has to exhibit the expected orbital symmetry, as proved by a specific photon polarization dependence in the isochromat spectrum. One also finds generally a much stronger temperature sensitivity for surface features as compared to bulk bands. This is the consequence of the larger vibration amplitudes in the selvedge region and the concomitant increased thermally induced disorder. Last, but not least, surface bands must only depend on \mathbf{k}_\parallel and not on k_\perp , the wave-vector component normal to the surface. The latter test requires the variation of $\hbar\omega$ over appreciable energy intervals and could therefore not be applied in the present work. Additional criteria are applicable to image-potential states. According to Sec. II, they are pinned to the vacuum level. The wave function of the $n \geq 1$ states peaks far outside the surface region and should, in contrast to crystal-induced and bulk states, show only weak dependence on the crystal temperature. This temperature insensitivity has in fact been demonstrated in a study of the $n \geq 1$ feature on Cu(100).³⁶ Concomitant with the low probability density of an image-potential state near the surface is its often-observed persistence upon gas adsorption. This property may be exploited to confirm the pinning to E_V . A clear-cut example is given in Fig. 6. The left-hand panel shows the image-potential states on clean Cu(100) as a step near $E - E_F = 4$ eV. After adsorption of half a monolayer of chlorine, the work-function increase of $\Delta\phi = 1.1$ eV shifts E_V . Consequently, all of the $n \geq 1$ barrier states are shifted by the same amount.³⁶ The same effect with opposite sign is shown in the right-hand panel of Fig. 6. The image-potential states appear near 5 eV on Pt(111). Adsorption of a small amount of potassium lowers the work

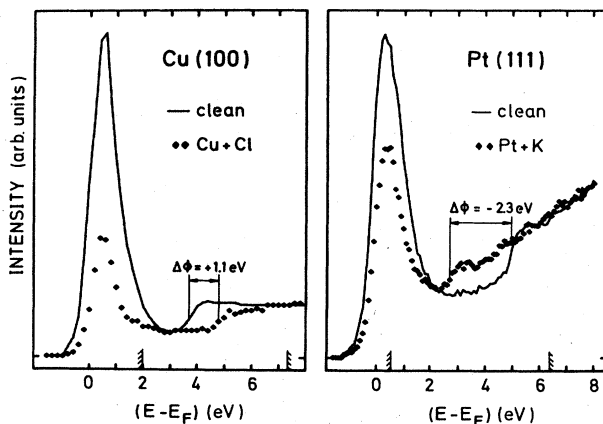


FIG. 6. Normal-incidence inverse photoemission spectra from Cu(100) and Pt(111) for clean and adsorbate-covered surfaces. Note the vacuum-level pinning of the image-potential-state emission.

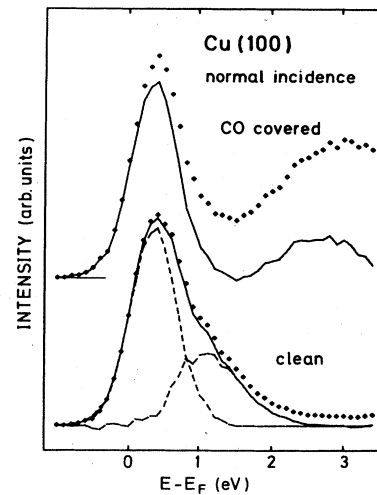


FIG. 7. Inverse photoemission spectrum from clean and CO-covered Cu(100). CO adsorption leads to a quenching of a surface resonance located at the high-energy side of the bulk-interband transition.

function by $\Delta\phi = -2.3$ eV. The resulting shift of the image-potential states is clearly demonstrated.³⁷

IV. DISCUSSION

Inspection of Fig. 2 reveals the common features of surface bands observed on the (100) surfaces. In every case, an image-potential state labeled S_1 starts at $\bar{\Gamma}$ less than 1 eV below the vacuum level (arrow labeled V). No crystal-induced surface state within the projected bulk band gap at $\bar{\Gamma}$ could be observed. Transitions B into bulk bands are indicated by the dashed-dotted lines. Off normal, along $\bar{\Gamma}\bar{X}$, the S_1 bands disperse upwards and finally disappear when crossing the boundary of the projected gap. This is to be expected, since Eq. (2) can then no longer be satisfied. However, new surface bands labeled S_2 are resolved when approaching \bar{X} , which of course cannot be understood within the simple scheme introduced in Sec. II. Systematic trends and analogies are also clearly seen in the results obtained for the corresponding (111) faces, see Fig. 3, and the (110) planes, see Fig. 4. In the following we will try to discuss these observations in more detail.

Image-potential states have been clearly identified at $\bar{\Gamma}$ on all (100) and (111) surfaces. Some of them have also been studied by other authors and we summarize the available information in Table I. Good agreement between the data of different groups is found. The binding energies are all well within the $E_V - E_1 \leq 1$ eV limit estimated by the model of Sec. II. We conclude that the energies at $\bar{\Gamma}$ are well understood, particularly, if the present-day experimental accuracy is also considered. One must keep in mind, in the latter context, that both the correct determination of E_F with the subsequent positioning of E_V in an isochromat spectrum and the correct identification of the ($n=1$)-level energy are clearly subject to experimental errors.

Off normal, the one-dimensional model is no longer applicable. In the simplest approximation, one may assume that the electronic motion in directions parallel to the surface will again be free-electron-like. This predicts a dispersion according to

$$E(\mathbf{k}_{\parallel}) = E_V - E_n + \hbar^2 k_{\parallel}^2 / 2m^*, \quad n \geq 1$$

with the effective electron mass m^* equal to the electron rest mass m . However, inspection of Table I clearly suggests the trend that $m^* > m$. Different reasons may be responsible for that. For example, surface corrugation was claimed recently⁵¹ to explain the observed m^* values. We will comment on this problem in Sec. V. Two remarks should be added for clarity. First, the distance at which the barrier-induced states attain their maximum probability density depends on n . The influence of surface corrugation is thus expected to become progressively less important and we expect $m^* \rightarrow m$ when $n \rightarrow \infty$. The experimental results of Table I, however, are clearly dominated by the $n=1$ intensity.⁸ It might be very interesting to study m^* in its dependence on n to help decide whether corrugation is an important factor. This goal has to be postponed, however, to future high-resolution experiments. Echenique and Pendry⁸ have given evidence that the intrinsic width of the $n > 1$ members of the Rydberg-like series decreases with n such that they should, in principle, be resolvable.

The surface bands S_1 on Cu(111) and Ag(111) tend to

TABLE I. Summary of surface-state data at $\bar{\Gamma}$ on different crystal faces. ϕ is the sample work function, $E_V - E_1$ the energy of the $n=1$ barrier-induced state, and m^*/m its dispersion at $\bar{\Gamma}$. The energy of the crystal-induced $n=0$ state is given with respect to E_F .

Sample	ϕ (eV)	Barrier induced		Crystal induced
		$(E_V - E_1)$ (eV)	m^*/m	$(E_0 - E_F)$ (eV)
Ni(100)	5.2 ^a	0.4 \pm 0.2 ^b 0.9 ^c	1.2 \pm 0.2 ^b	?
Cu(100)	4.59 ^d	0.6 \pm 0.2 ^e 0.64 ^h	1.2 \pm 0.2 ^f	+ 1.1 ^g
Ag(100)	4.6 ⁱ	0.5 \pm 0.2 ^j 0.5 ^k	1.2 \pm 0.2 ^j 1.6 \pm 0.3 ^k	?
Ni(111)	5.2 ^l	0.6 \pm 0.2 ^b	1.6 \pm 0.2 ^b	-0.2 ^{l,m}
Cu(111)	4.98 ^d	0.8 \pm 0.2 ⁿ 0.94 \pm 0.1 ^q	1.2 \pm 0.2 ⁿ 1 ^q	-0.4 ^{o,p}
Ag(111)	4.74 ⁱ	0.6 \pm 0.2 ^j	1.4 \pm 0.3 ^j	-0.1 ^r
Ni(110)	5.04 ^d	0.6 \pm 0.3 ^b	1.7 \pm 0.3 ^b	

^aReference 38.

^bReference 10.

^cReference 41.

^dReference 39.

^eReference 12.

^fReference 36.

^gReference 44.

^hReference 42.

ⁱReference 40.

^jReference 34.

^kReference 43.

^lReference 45.

^mReference 46.

ⁿReference 35.

^oReference 47.

^pReference 48.

^qReference 49.

^rReference 50.

leave the projected bulk band gap but still survive, in contrast to the model expectation. We think this is no contradiction. On the one hand, the experimental error bars and the inaccuracies, which the parameters used to calculate projected gaps are known to have, are still compatible with an "in-gap" position. On the other hand, and perhaps more important from a basic point of view, calculations of the electron transmission function T near gap edges clearly show that T is not steplike at, e.g., the L_1 point but shows a delayed onset above L_1 and below L_2 . For example, the transmission at X_1 on Cu(100) attains its maximum amplitude only about 1 eV above X_1 .⁵² Consequently, the effective gap at X necessary to satisfy Eq. (2) of Sec. II is somewhat larger than the energy difference $E(X_1) - E(X_4)$ as calculated from the bulk-band parameters.

Next, we focus on the crystal-induced surface states predicted several eV below E_V at $\bar{\Gamma}$. Inspection of Figs. 3(b) and 3(c) suggests that we identify the $n=0$ states with the bands labeled S_2 . These are occupied at $\bar{\Gamma}$ and were observed already in earlier photoemission studies (compare Table I). Their observed Λ_1 symmetry⁵³ is fully compatible with the one-dimensional model. Away from $\bar{\Gamma}$ they disperse upwards and finally disappear at E_F . Photoemission data are plotted in Fig. 3 as small dots. Their continuation above E_F is clearly observed in our results (see bands labeled S_2 in Fig. 3). Figures 3(b) and 3(c) suggest that the isochromat spectra indicate that S_2 is also near $\bar{\Gamma}$, i.e., in the \mathbf{k}_{\parallel} region where S_2 is occupied. This is a mere consequence of our limited energy and angular resolution and is not in conflict with the proposed interpretation. The dispersion of S_2 below E_F on Cu(111) is characterized by an effective mass of $m^*/m = 0.42$.⁴⁸ Its extension above E_F yields $m^*/m = 0.7 \pm 0.3$, compatible with the photoemission result. On Ag(111) we obtain $m^*/m = 1.0 \pm 0.2$ from our results above E_F . No photoemission result is available for comparison. The situation is more complex on Ni(111). Here, the majority- and minority-spin systems give rise to different electron states. An extensive discussion of the Ni(111)-surface states in the context of detailed numerical calculations within the one-step model of inverse photoemission will be published elsewhere.⁴⁶ Therefore, we summarize here only the main results relevant in the present context. The L_2-L_1 gap extends from $E - E_F = -0.9$ eV to about +6.5 eV. However, in contrast to the situation found at L in Cu and Ag, the L_{31} point is located within this gap [compare Fig. 3(a)]. If we neglect this fact— L_3 is of different symmetry and cannot mix into the L_2-L_1 gap states at $\bar{\Gamma}$ —the one-dimensional model of Sec. II predicts one $n=0$ Shockley state. We identify this state with the occupied Λ_1 band labeled S_3 in Fig. 3(a). It was observed earlier in photoemission studies⁴⁵ at about -0.2 eV at $\bar{\Gamma}$. The result of our calculation⁴⁶ is indicated by a dashed line and reproduces quite well both its energetic position at $\bar{\Gamma}$ and the downward dispersion with increasing k_{\parallel} . The band labeled S_2 in Fig. 3(a) dispersing towards higher energies falls in a region of the projected bulk-band structure where bulk states of the same (even) parity may exist. The calculation⁴⁶ thus identifies S_2 as a surface resonance. The model of Sec. II allows only one crystal-

induced Shockley-type state in the L_2-L_1 gap. Consequently, S_2 should not persist at exactly $k_{\parallel}=0$. This cannot be resolved in our experiment, since S_2 merges into the bulk-band transitions labeled B in Fig. 3(a) and drawn by the dashed-dotted lines. However, the calculation in fact finds just the expected behavior, see the dashed line above S_2 .

In contrast to the (111) surfaces, the identification of the $n=0$ crystal-induced states appears to be more difficult on the (100) faces. The reason for this is that in all three cases studied here, a very prominent peak is observed slightly above E_F , which results from dipole-allowed $\Delta_1 \rightarrow \Delta_1$ bulk-band transitions.^{5,10,12,34,43} Their dispersion is indicated in Figs. 2(a)–2(c) by the dashed-dotted curves labeled B . This fact precludes so far the identification of $n=0$ states on Ni(100) and Ag(100). Contamination experiments at $\bar{\Gamma}$ on Ni(100) show an appreciable sensitivity of the bulk peak, a result not in disagreement with the idea of an $n=0$ state superimposed on the bulk feature at about the same energy. However, we admit that this question can only be answered by an experiment employing a tunable photon detector to shift away the bulk-transition peak. The situation on Ag(100) is not clear either. Here, transition B observed at $\bar{\Gamma}$ exhibits a rather broad asymmetric shoulder at higher energy.^{34,43} However, both the shoulder and peak B respond sensitively to contamination, thus precluding a separation of bulk and surface emissions. A surface resonance was clearly identified⁴⁴ at 1.1 eV above E_F on Cu(100) [see the solid diamond plotted at $\bar{\Gamma}$ in Fig. 2(b)]. The basic result of this experiment⁴⁴ is reproduced in Fig. 7. Diamonds show the spectra as measured under otherwise identical conditions for clean and CO-covered Cu(100). The asymmetric shoulder observed at about 1.1 eV on clean Cu is quenched by the adsorbate. After linear background subtractions (solid curves), the clean Cu result can be decomposed (dashed curves) into the bulk contribution at 0.4 eV and the surface resonance at 1.1 eV. It seems quite natural to identify this surface resonance with the $n=0$ prediction of the one-dimensional model. In fact, the experiment places the surface resonance about 0.8 eV below the lower gap edge at X_4 . We would like to recall here that gap edges do not depend in a steplike manner on energy (see the discussion above). The observed Δ_1 -like symmetry of the surface resonance¹² also supports the $n=0$ identification. Finally, our interpretation could be substantiated by recent one-step-model calculations, which predict a surface resonance of Δ_1 symmetry about 1.8 eV above E_F at $\bar{\Gamma}$.⁴⁴

Next, we discuss the remaining bands in Fig. 2. They are obviously connected with the gap around \bar{X} . This gap is essentially the projection of the L_2-L_1 gap onto the (100) face. The corresponding geometry in k space is evident from Fig. 5. Clearly, the one-dimensional two-band model cannot account for surface states near \bar{X} . However, one may expect crystal-induced Shockley states near E_F in close analogy to those reported on the (111) faces. In fact, photoemission from Cu(100) resolves such a band at -0.058 ± 0.005 eV at \bar{X} , with an effective mass of $m^*/m = 0.067$.⁵⁴ It is indicated by the small dots in Fig. 2(b). Evidence for an analogous band near \bar{X} on Ag(100)

is given in recent electroreflectance experiments,⁵⁵ which suggest its extension above E_F . The dashed line near E_F at \bar{X} in Fig. 2(c) reproduces the result of a corresponding numerical calculation.⁵⁵ An occupied surface state at \bar{X} on Ag(100) has not been resolved yet. We mention, however, that the analogous band on Au(100) was clearly identified⁵⁶ in photoemission. The existence of such a band near the bottom of the \bar{X} gap thus seems to be a quite general feature of (100) fcc surfaces and will probably also be predicted for Ni(100). Unfortunately, the low $\hbar\omega$ of our experiments limits the available k_{\parallel} range and does not allow us to reach the bottom of the \bar{X} gap in all three cases of Fig. 2.

The bands labeled S_2 in Fig. 2 are electron states derived from the upper edges of the projected bulk band gaps. The S_2 band on Cu(100) exhibits an effective mass of $m^*/m = 1.2 \pm 0.2$ when extrapolated to \bar{X} . It closely follows the upper boundary of the gap. Its position and dispersion would be well explained by a recent one-step-model calculation.³² The two dashed lines in Fig. 2(b), which enclose the S_2 band, are numerical results of Dose *et al.*³² for two different positions of a steplike surface-potential barrier. The S_2 band on Ag(100) was also observed recently by Reihl *et al.*⁴³ They determined its energy to be 3.8 ± 0.4 eV, but were not able to resolve any dispersion away from \bar{X} . Our results give an energy of 3.5 ± 0.2 eV above E_F at \bar{X} . An energy of 3.1 eV is given by recent electroreflectance results.⁵⁵ The dashed line below S_2 in Fig. 2(c) reproduces the theoretical band obtained in Ref. 55. This calculation reproduces both the energy and dispersion of S_2 quite accurately. An analogous band at $\bar{X} = 2.6$ eV was also found in a study of electroreflectance from Au(100).⁵⁷ Thus, the observed systematic trends explain the S_2 on Ni(100), for which no calculations are available yet. Finally, we mention that the observed bulk bands labeled B in Fig. 2 systematically tend to shift into the projected gap for the largest k_{\parallel} values. It is tempting to connect the large k_{\parallel} points of B with the surface bands observed near \bar{X} at the bottom of the gaps. The extrapolated bands running parallel to the gap boundary would then represent a quite general class of Tamm-like surface states. However, this prediction must await new experiments at larger k_{\parallel} values.

Finally, we discuss the surface emissions observed on the (110) crystal faces (see Fig. 4). Since there is no gap at $\bar{\Gamma}$, we expect no barrier-induced states. This is indeed true for Ni and Ag. However, on Ni the extension of such a state (labeled S_1) to larger k_{\parallel} values inside the projected gap is clearly resolved. Its extrapolation to $k_{\parallel}=0$ yields a binding energy of 0.6 ± 0.3 eV and an effective mass $m^*/m = 1.7 \pm 0.3$. These results are compatible with the results obtained on the (100) and (111) surfaces. Rather faint steps in the isochromat spectra are observed on Cu(110), even at $\bar{\Gamma}$, and their position is indicated by the open circles labeled S_1 in Fig. 4(b). This is probably an image-potential state also. However, the error bars do not allow the precise determination of its energy and dispersion. Surface states of the gap-induced Shockley type S_2 may also be expected well inside the gap around \bar{Y} . They show up as very prominent emission features in the experimental spectra. Results similar to ours have been found

for Cu(110),⁵⁸ at 2.5 eV above E_F at \bar{Y} , and for Ag(110),⁵⁹ at 1.65 eV above E_F at \bar{Y} . Our data give 1.8 ± 0.2 and 1.6 ± 0.2 eV, respectively. The dashed lines plotted along S_2 in Figs. 4(b) and 4(c) are results from early numerical calculations.^{60,61} The data for Cu(110) (Ref. 60) were obtained from an extended Hückel study, the parameters of which were derived from the well-known Cu bulk bands. The data for Ag(110) (Ref. 61) are due to a first-principles, self-consistent pseudopotential calculation of the surface electronic structure. We note an almost perfect agreement with the experimental results in both cases. No calculations are available for the S_2 band on Ni(110). The solid line in Fig. 4(a) is a parabolic fit to the data points which yielded an energy of $E - E_F = 2.6$ eV at \bar{Y} and $m^*/m = 0.5$. Figure 5 reveals that \bar{Y} is also related to the L -point gap. One may therefore expect Shockley-type states also near the bottom of the \bar{Y} gap. One such state has been observed recently on Cu(110) by photoemission experiments⁶² at 0.4 eV below E_F at \bar{Y} and with $m^*/m = 0.26$. It is plotted in Fig. 4(b) by small dots, labeled S_3 . The corresponding dashed line is taken from the calculation reported in Ref. 60. A bulk-band transition labeled B on Cu(110) between $\bar{\Gamma}$ and \bar{Y} is clearly identified for $k_{\parallel} \leq 0.6 \text{ \AA}^{-1}$ (Ref. 35). However, for larger k_{\parallel} values it extends into the projected bulk band gap. In this region the observed data points probably represent the extension of the occupied S_3 band above E_F . An occupied band in analogy to S_3 has also been recently identified 0.1 eV below E_F at \bar{Y} on Ag(110).⁶³ An analogous occupied band was detected at \bar{Y} on Au(110).⁵⁶ This suggests again a systematic trend, probably also including Ni(110). A similar trend is observed on the (110) faces around \bar{X} . Only one calculation of a surface band is available. It refers to Ag(110) (Ref. 61) and is shown in Fig. 4(c) as a dashed line. It is lower in energy by about 0.8 eV than the experimental result, but reproduces the observed dispersion quite accurately. No calculations are known to

us for Ni and Cu around \bar{X} . In these cases solid lines represent parabolic fits to the data points. Note that both on Ni and Cu, bulk-band transitions approach the boundaries of the \bar{X} gap near its bottom in such a way that they might well become surface resonances and/or surface bands there. To clarify this point, experiments with tunable photon energy seem to be mandatory. The considerable number of surface bands observed up to now in the \bar{X} gap of the (100) surfaces and in both the \bar{Y} and \bar{X} gaps of the (110) surfaces are characterized by their energy positions at \bar{X} or \bar{Y} , respectively, and their band dispersions represented by an effective mass. These data are collected in Table II.

V. SUMMARY AND OUTLOOK

We have studied angle-resolved inverse photoemission spectra from the (100), (110), and (111) surfaces of Ni, Cu, and Ag over extended energy and angular intervals. The present paper is devoted almost exclusively to the wealth of surface bands observed in our work and by previous authors. All surface bands could be classified as being either induced by the image-potential barrier outside the metal surface, or as being intimately related to the evanescent wave functions in bulk band gaps.

Image-potential states should occur on all metals, provided they are located energetically within a gap of the projected bulk-band structure. This gap prevents the electrons from penetrating into the crystal and traps them outside the surface. We could identify image-potential states on the (100) and (111) faces of all three metals and on the (110) face of Ni. They are bound by less than 1 eV with respect to the vacuum level. The corresponding Rydberg-like series could not be resolved experimentally. When going off normal the $n = 1$ members of this series, which dominate the spectra in intensity, exhibit effective masses m^*/m generally greater than or equal to 1.

Effective masses $m^*/m > 1$ have been recently attributed to surface corrugation.⁵¹ Corrugation will of course contribute to m^* in principle. It was treated in Ref. 51 in a truncated second-order perturbation theory. The validity of such an approach is questionable in view of the large observed effective masses. Moreover, the fact that we observe equal effective masses on Ni(111) and Ni(110) but a smaller one on Ni(100) is in clear contradiction to the simple corrugation argument.

Tamm-type surface states of d -orbital character could not be identified in the present work. However, many Shockley-type surface bands are observed in the gaps at $\bar{\Gamma}$ on the (111) surfaces and in both the gaps around \bar{X} and \bar{Y} on the (110) surfaces. A surface resonance could also be resolved on Cu(100), just below the gap edge at $\bar{\Gamma}$. All bulk gaps relevant in the present work are of the Shockley inverted type. We conclude that in all of the corresponding projected surface gaps at least one surface band exists. The results at \bar{X} and \bar{Y} on the (110) surfaces suggest that the appearance of two sp -like surface bands, one at about midgap and one near the bottom of the gap, may be a general feature of the class of metals under consideration. Comparison to available numerical calculations shows that the crystal-induced (Shockley-type) surface-band en-

TABLE II. Summary of surface-state data at \bar{X} and \bar{Y} on the (110) surfaces and at \bar{X} on the (100) surfaces. $E - E_F$ is the energetic position above E_F and m^*/m the dispersion at the respective symmetry point.

Sample	$(E - E_F)$ (eV)	m^*/m	Ref.
Ni(110) at \bar{Y}	2.6 ± 0.2	0.5 ± 0.1	10
Cu(110) at \bar{Y}	1.8 ± 0.2	0.8 ± 0.2	35
	2.5 ± 0.2	1.1	58
Ag(110) at \bar{Y}	1.6 ± 0.2	0.9 ± 0.2	34
	1.65		59
Ni(110) at \bar{X}	6.5 ± 0.3	2.2 ± 0.3	10
Cu(110) at \bar{X}	5.4 ± 0.3	2.0 ± 0.2	35
Ag(110) at \bar{X}	5.0 ± 0.2	2.0 ± 0.4	34
Ni(100) at \bar{X}	5.5 ± 0.3^a	2.0 ± 0.4	10
Cu(100) at \bar{X}	3.8 ± 0.2^a	1.2 ± 0.2	32
Ag(100) at \bar{X}	3.5 ± 0.2	0.6 ± 0.2	34
	3.8 ± 0.4		43

^aExtrapolated to \bar{X} , compare Figs. 2(a) and (b).

ergies generally agree to better than 1 eV and that the predicted dispersions reproduce the experimental observations quite well.

The theoretical treatment of image-potential states on the other hand is much less satisfactory. A local-density pseudopotential calculation,^{55,57} which describes crystal-induced surface states quite accurately, fails to give any indication of image-potential states. This is of course a consequence of the incorrect asymptotic form of the surface potential. For a simultaneous correct description of both crystal-induced and image-potential-induced surface states, improved models of the surface potential barrier

are needed. The wealth of surface-state data now known will certainly facilitate the construction of such models.

Note added in proof. Another paper by Dempsey, Grise, and Kleinman has come to our attention after submission of the manuscript.⁶⁴ It contains calculated surface bands on nickel which agree very well with our data labeled S_2 on Ni(001) in Fig. 2 and S_2 on Ni(110) in Fig. 4.

ACKNOWLEDGMENTS

This work was financially supported by the Deutsche Forschungsgemeinschaft.

- ¹F. J. Himpsel, *Adv. Phys.* **32**, 1 (1983).
- ²E. W. Plummer and W. Eberhardt, *Adv. Chem. Phys.* **46**, 533 (1982).
- ³R. Courths and S. Hüfner, *Phys. Rep.* **112**, 53 (1984).
- ⁴V. Dose, *Progr. Surf. Sci.* **13**, 225 (1983).
- ⁵D.-P. Woodruff, P. D. Johnson, and N. V. Smith, *J. Vac. Sci. Technol. A* **1**, 1104 (1983).
- ⁶F. J. Himpsel and Th. Fauster, *J. Vac. Sci. Technol. A* **2**, 815 (1984).
- ⁷V. Dose, *J. Phys. Chem.* **88**, 1681 (1984); in *Proceedings of the Third International Conference on Solid Films and Surfaces, Sydney, 1984* [*Appl. Surf. Sci.* (to be published)].
- ⁸P. M. Echenique and J. B. Pendry, *J. Phys. C* **11**, 2065 (1978); E. G. McRae, *Rev. Mod. Phys.* **51**, 541 (1979).
- ⁹D. P. Woodruff, N. V. Smith, P. D. Johnson, and W. A. Royer, *Phys. Rev. B* **26**, 2943 (1982).
- ¹⁰A. Goldmann, M. Donath, W. Altmann, and V. Dose, *Phys. Rev. B* **32**, 837 (1985).
- ¹¹G. Thörner and G. Borstel, *Solid State Commun.* **47**, 329 (1983).
- ¹²W. Altmann, V. Dose, A. Goldmann, U. Kolac, and J. Rogozik, *Phys. Rev. B* **29**, 3015 (1984).
- ¹³I. Tamm, *Z. Phys.* **76**, 848 (1932).
- ¹⁴S. G. Davison and J. D. Levine, in *Solid State Physics*, edited by H. Ehrenreich, F. Seitz, and D. Turnbull (Academic, New York, 1970), Vol. 25, p. 1.
- ¹⁵A. W. Maue, *Z. Phys.* **94**, 717 (1935).
- ¹⁶E. T. Goodwin, *Proc. Cambridge Philos. Soc.* **35**, 205 (1935).
- ¹⁷W. Shockley, *Phys. Rev.* **56**, 317 (1939).
- ¹⁸F. Forstmann, *Z. Phys.* **235**, 69 (1970).
- ¹⁹J. B. Pendry and S. J. Gurman, *Surf. Sci.* **49**, 87 (1975).
- ²⁰P. Heimann, J. Hermanson, H. Miosga, and H. Neddermeyer, *Phys. Rev. B* **20**, 3059 (1979), and references therein.
- ²¹R. G. Jordan and G. S. Sohal, *J. Phys. C* **15**, L663 (1982).
- ²²H. Asonen, M. Lindroos, M. Pessa, R. Prasad, R. S. Rao, and A. Bansil, *Phys. Rev. B* **25**, 7075 (1982).
- ²³D. Westphal and A. Goldmann, *Surf. Sci.* **95**, L249 (1980).
- ²⁴A. Goldmann and E. Bartels, *Surf. Sci.* **122**, L629 (1982).
- ²⁵P. Heimann, J. Hermanson, H. Miosga, and H. Neddermeyer, *Phys. Rev. Lett.* **43**, 1757 (1979).
- ²⁶F. J. Arlinghaus, J. G. Gay, and J. R. Smith, *Phys. Rev. B* **23**, 5152 (1981), and references therein.
- ²⁷E. G. McRae, *J. Vac. Sci. Technol.* **16**, 654 (1979).
- ²⁸D. S. Boudreaux and V. Heine, *Surf. Sci.* **8**, 426 (1967).
- ²⁹C. Kittel, *Introduction to Solid State Physics*, 5th ed. (Wiley, New York, 1974).
- ³⁰J. K. Greppstadt, B. J. Slagsvold, and I. Bartos, *J. Phys. F* **12**, 1679 (1982).
- ³¹K. Desinger, V. Dose, M. Glöbl, and H. Scheidt, *Solid State Commun.* **49**, 479 (1984).
- ³²V. Dose, U. Kolac, G. Borstel, and G. Thörner, *Phys. Rev. B* **29**, 7030 (1984).
- ³³W. Altmann, M. Donath, V. Dose, and A. Goldmann, *Solid State Commun.* **53**, 209 (1985).
- ³⁴W. Altmann *et al.* (unpublished).
- ³⁵W. Jacob *et al.* (unpublished).
- ³⁶V. Dose, W. Altmann, A. Goldmann, U. Kolac, and J. Rogozik, *Phys. Rev. Lett.* **52**, 1919 (1984).
- ³⁷J. Rogozik *et al.* (unpublished).
- ³⁸W. Eib and S. F. Alvarado, *Phys. Rev. Lett.* **37**, 444 (1976).
- ³⁹J. Hölzl and F. K. Schulte, *Springer Tracts in Modern Physics* (Springer, Berlin, 1979), Vol. 85.
- ⁴⁰M. Chelvayohan and C. H. B. Mee, *J. Phys. C* **15**, 2305 (1982).
- ⁴¹P. D. Johnson and N. V. Smith, *Phys. Rev. B* **27**, 2527 (1983).
- ⁴²D. Straub and F. J. Himpsel, *Phys. Rev. Lett.* **52**, 1922 (1984).
- ⁴³B. Reihl, K. H. Frank, and R. R. Schlittler, *Phys. Rev. B* **30**, 7328 (1984).
- ⁴⁴G. Thörner, G. Borstel, V. Dose, and J. Rogozik, *Surf. Sci.* (to be published).
- ⁴⁵F. J. Himpsel and D. E. Eastman, *Phys. Rev. Lett.* **41**, 507 (1978).
- ⁴⁶G. Borstel, G. Thörner, M. Donath, V. Dose, and A. Goldmann, *Solid State Commun.* (to be published).
- ⁴⁷P. O. Gartland and B. J. Slagsvold, *Phys. Rev. B* **12**, 4047 (1975); P. Heimann, J. Hermanson, H. Miosga, and H. Neddermeyer, *Surf. Sci.* **85**, 263 (1978).
- ⁴⁸S. D. Kevan, *Phys. Rev. Lett.* **50**, 526 (1983).
- ⁴⁹N. V. Smith, in *Proceedings of the Third International Conference on Solid Films and Surfaces, Sydney, 1984* [*Appl. Surf. Sci.* (to be published)].
- ⁵⁰H. F. Roloff and H. Neddermeyer, *Solid State Commun.* **21**, 561 (1977); G. V. Hanson and S. A. Flodström, *Phys. Rev. B* **17**, 473 (1978).
- ⁵¹N. Garcia, B. Reihl, K. H. Frank, and A. R. Williams, *Phys. Rev. Lett.* **54**, 591 (1985).
- ⁵²K. K. Kleinherbers, A. Goldmann, E. Tamura, and R. Feder, *Solid State Commun.* **49**, 735 (1984).
- ⁵³A. Goldmann, D. Westphal, and R. Courths, *Phys. Rev. B* **25**, 2000 (1982).
- ⁵⁴S. Kevan, *Phys. Rev. B* **28**, 2268 (1983).
- ⁵⁵D. H. Kolb, W. Boeck, Kai-Ming Ho, and S. H. Liu, *Phys. Rev. Lett.* **47**, 1921 (1981).
- ⁵⁶P. Heimann, H. Miosga, and H. Neddermeyer, *Phys. Rev. Lett.* **42**, 801 (1979).
- ⁵⁷W. Boeck and D. M. Kolb, *Surf. Sci.* **118**, 613 (1982).
- ⁵⁸R. A. Bartynski, T. Gustafson, and P. Soven, *Phys. Rev. B* **31**, 4745 (1985).
- ⁵⁹B. Reihl, R. R. Schlittler, and H. Neff, *Phys. Rev. Lett.* **52**,

- 1826 (1984).
- ⁶⁰B. G. Dempsey and L. Kleinmann, Phys. Rev. B **16**, 5356 (1977).
- ⁶¹Kai-Ming Ho, B. N. Harmon, and S. H. Liu, Phys. Rev. Lett. **44**, 1531 (1980).
- ⁶²S. Kevan, Phys. Rev. B **28**, 4822 (1983).
- ⁶³K. K. Kleinherbers, unpublished results.
- ⁶⁴D. G. Dempsey, W. R. Grise, and Leonard Kleinman, Phys. Rev. B **18**, 1270 (1978).